Journal of Materials processing Technology, Vol 153-154, 2004, pp. 488-493.

A study of abrasive waterjet characteristics by CFD simulation

H. Liu[1], J. Wang[1], N. Kelson[2] and R.J. Brown[1]
1. School of Mechanical, Manufacturing and Medical Engineering, Queensland University of Technology, GPO Box 2434, Brisbane, QLD 4001, Australia; email h3.liu@qut.edu.au
2. HPC/AMAC School of Mathematical Sciences, Queensland University of Technology, GPO Box 2434, Brisbane, QLD 4001, Australia;

ABSTRACT

Computational Fluid Dynamics (CFD) models for ultrahigh velocity waterjets and abrasive waterjets (AWJs) are established using the Fluent6 flow solver. Jet dynamic characteristics for the flow downstream from a very fine nozzle are then simulated under steady state, turbulent, two-phase and three-phase flow conditions. Water and particle velocities in a jet are obtained under different input and boundary conditions to provide an insight into the jet characteristics and a fundamental understanding of the kerf formation process in AWJ cutting. For the range of downstream distances considered, the results indicate that a jet is characterized by a decay of the axial velocity at the jet centre and there is a rapid evolution from the inlet conditions to a top-hat velocity profile downstream.

KEYWORDS: Abrasive waterjet, CFD, Multiphase axisymmetric flow, Jet characteristics

1. INTRODUCTION

Abrasive waterjet (AWJ) technology is a state-of-the art cutting tool used to machine a wide range of metals and non-metals, particularly ‘difficult-to-cut’ materials such as ceramics and marbles [1-3], and layered composites [3-6]. AWJ machining includes AWJ slotting, turning, drilling and milling [7]. Compared with the traditional and other non-traditional machining methods, the AWJ cutting technology has a number of distinct advantages, such as no thermal distortion, high machining versatility, ability to produce contours, good surface quality, easy integration with mechanical manipulators, and minimal burrs [8].

Typically, an abrasive waterjet system includes the following components: a special high-pressure pump or intensifier, a water catching unit, a nozzle positioning system, an abrasive delivery system, and a mixing unit made of an orifice, a mixing chamber and a focus nozzle. The commonly used or conventional AWJ machines are entrainment abrasive waterjet systems in which water is pumped to a very high pressure by using an intensifier technology. This high-pressure water then flows through an orifice to form a very high velocity jet of water. As the water jet passes through the mixing chamber, abrasive particles are sucked into the mixing chamber through a separate inlet due to the vacuum created by the water jet. The turbulent process in the mixing chamber causes the water and particles to mix and form a very powerful abrasive waterjet. By transferring the momentum between water and abrasive particles in the narrow focus nozzle, high velocity streams of abrasives are formed with great cutting capabilities.

Since the introduction of AWJ cutting technology, a large amount of research and development effort has been made to explore its applications and associated science [9].

However, this technology is still under flux and development. Its many aspects are yet to be fully understood. Specifically, an understanding of the hydrodynamic characteristics (e.g. velocity and pressure distributions) of an abrasive waterjet is essential for improving nozzle design, as well as for modelling, evaluating and improving AWJ cutting performance. However, this work has proved to be complicated. For example, the water-particle interaction in the mixing unit is extremely intricate while the ultrahigh velocity and small nozzle and particle dimensions make the investigation of the jet and particle behaviour difficult. Nevertheless, some important investigations have been reported on understanding the AWJ dynamic characteristics for relatively low velocity AWJs and for particular jet cutting status through theoretical [10, 11] and experimental [12, 13] studies as well as CFD simulation [14, 15]. However, research on ultrahigh pressure waterjets and abrasive waterjets to arrive at a comprehensive understanding of the jet properties has received little attention [3,16].

The present work is to gain a fundamental knowledge of the ultrahigh velocity jet dynamic characteristics such as the velocity distribution. This knowledge is essential for enhancing the AWJ cutting technology, understanding the kerf formation or cutting process and modelling the various cutting performance measures that are required for process control and optimization. For this purpose, CFD analysis is found to be a viable approach because direct measurement of particle velocities and visualization of particle trajectories are very difficult for the ultrahigh speed and small dimensions involved. In this paper, CFD models for ultrahigh velocity waterjets and abrasive waterjets are established using the Fluent6 flow solver [17]. Jet dynamic characteristics such as the water and particle velocities for the flow downstream from a very fine nozzle are then simulated under steady state, turbulent, two-phase and three-phase flow conditions and a range of inlet conditions and input parameters. The results from the CFD study are then analysed to gain an insight into the jet characteristics and a fundamental understanding of the kerf formation process in ultrahigh velocity AWJ cutting.

2. MODEL FORMULATION

The major governing equations used to form the CFD model and the boundary conditions for the stimulation study are given below.

2.1 Governing equations

The multiphase volume of fluid (VOF) model available in Fluent6 is chosen to simulate the present flows. Initially, the CFD model considers two-phase (air and water) flow, where air is treated as the primary phase. A resume of the relevant equations in Cartesian tensors is given below.

The continuity equation for the volume fraction of q^{th} phase is

$$\frac{\partial \alpha_q}{\partial t} + u_i \frac{\partial \alpha_q}{\partial x_i} = 0 \tag{1}$$

where α_q donates the qth phase volume fraction, u_i represents the velocities in the x_i coordinate directions and t is time. The volume fraction equation is not solved for the primary phase, instead the primary-phase volume fraction is computed based on the constraint that the sum of the volume fractions of all phases is one.

The momentum equation [18] is solved throughout the domain, and the resulting velocity field is shared among the phases:

$$\frac{\partial}{\partial t}\rho u_i + \frac{\partial}{\partial x_j}\rho u_i u_j = -\frac{\partial P}{\partial x_i} + \frac{\partial}{\partial x_j}\mu\left(\frac{\partial u_i}{\partial x_j} + \frac{\partial u_j}{\partial x_i}\right) + \frac{\partial}{\partial x_j}\left(-\rho\overline{u_i' u_j'}\right) \tag{2}$$

where x_i and x_j are coordinate directions, u_i represents the velocities in the x_i coordinate directions, u_j represents the velocities in the x_j coordinate directions, P is the static pressure, ρ is the constant density, μ is the dynamic viscosity, $\overline{u_i' u_j'}$ is the Reynolds stress. The properties appearing in the governing equations are determined by the presence of the component phases in each control volume. In this system, for example, if the density of air and water phases are represented by the subscripts ρ_1 and ρ_2, and if the volume fraction of water is being tracked, the density in each cell is given by $\rho = \alpha_2\rho_2 + (1-\alpha_1\rho_1)$. The dynamic viscosity is also computed in this manner.

The transport equations for the turbulence energy k and dissipation rate ε are solved, and shared by the phases throughout the field. The standard k-ε model [19] is chosen in this simulation work. This model is mathematically given by

$$\frac{\partial}{\partial t}(\rho k) + \frac{\partial}{\partial x_i}(\rho k u_i) = \frac{\partial}{\partial x_i}\left[\left(\mu + \frac{\mu_t}{\sigma_k}\right)\frac{\partial k}{\partial x_i}\right] + G_k - \rho\varepsilon \tag{3}$$

$$\frac{\partial}{\partial t}(\rho \varepsilon) + \frac{\partial}{\partial x_i}(\rho \varepsilon u_i) = \frac{\partial}{\partial x_i}\left[\left(\mu + \frac{\mu_t}{\sigma_\varepsilon}\right)\frac{\partial \varepsilon}{\partial x_i}\right] + C_{1\varepsilon}\frac{\varepsilon}{k}G_k - C_{2\varepsilon}\rho\frac{\varepsilon^2}{k} \tag{4}$$

where $\mu_t = \rho C_\mu \frac{k^2}{\varepsilon}$ is the turbulent viscosity, G_k is the generation of turbulent kinetic energy due to the mean velocity gradients, u_i represents the velocities in the x_i coordinate directions, C_μ, $C_{1\varepsilon}$, $C_{2\varepsilon}$ are constant, σ_k and σ_ε are the turbulent Prandtl numbers for k and ε respectively, and ρ and μ are as defined earlier. The values of the constants are taken from [19], i.e. C_μ =0.09, $C_{1\varepsilon}$ =1.44, $C_{2\varepsilon}$ =1.92, σ_k=1, and σ_ε= 1.3.

The effect of particles on the continuum is neglected in this study, as are the particle-particle interactions. Fluent calculates particle trajectories by integrating the force balance on each particle, which includes the particle inertia and drag force, and for a single particle, the force balance equation can be written as

$$\frac{du_p}{dt} = F_D(u - u_p) \tag{5}$$

where u is the fluid phase velocity, u_p is the particle velocity, and $F_D(u-u_p)$ is the drag force per unit particle mass that is given by

$$F_D = \frac{18\mu}{\rho_p D_p^2}\frac{C_D R_e}{24} \tag{6}$$

in which ρ_p is the density of particle (garnet is used in this study), D_p is the particle diameter, R_e is relative Reynolds number, and C_D is the drag coefficient given by

$$C_D = a_1 + \frac{a_2}{R_e} + \frac{a_3}{R_e^2} \tag{7}$$

where the *a*'s are constants that apply for smooth spherical particles over several ranges of *Re* and their values are given by Morsi and Alexander [20].

These general governing equations are then converted into their polar coordinate forms and used for steady state, turbulent, incompressible, two-phase axisymmetric flows. A control-volume-based technique is used to convert the governing equations to algebraic equations that can be solved numerically. After the solution of pure water jets has been completed, particle motions and trajectories are solved using the Discrete Phase Model [17], where a three-phase (water, air and particles) axisymmetric flow is considered.

2.2 Boundary conditions and solution methodology

The geometry of computational domain with boundary conditions is shown in Figure 1. A pure waterjet is considered as a two-dimensional, steady axisymmetric turbulent flow that has passed through a long thin nozzle attached to the mixing chamber before entering the atmosphere as a free jet. Because the jet is assumed to be axisymmetric, symmetry conditions are applied along AE and only the upper half of flow domain was solved. The CFD simulation starts where the jet exits the nozzle and enters the computational domain across the boundary AB, and ends after the jet has travelled 50mm downstream. In the absence of experimental data, the flow at the nozzle exit is assumed to be fully developed to a $1/7^{th}$ power law distribution for the mean velocity profile [21]. Across AB, the default solver values for the turbulent kinetic energy and dissipation rate are used, and the liquid volume fraction is set to one over this boundary. In addition, the waterjet in the inlet AB is assumed to have a negligible velocity defect for the particles. In the CFD model, section BC is treated as a slip wall, whereas sections CD and DE as shown in Figure 1 are considered as free boundaries for which pressure inlet conditions are used. Also, it is expected that only air will be entrained into the computational domain; therefore, the air volume fraction for any fluid *entering* the domain across CD or DE is set to unity.

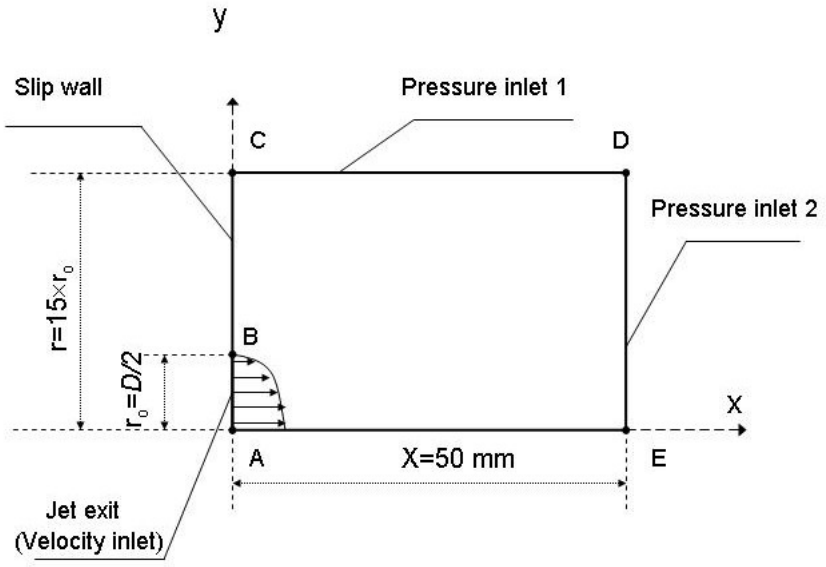

Figure 1. Computation domain and boundary conditions of CFD model.

To investigate the accuracy, stability and convergence properties of the CFD model, a number of initial computations were performed using a 2^{nd} order convective discretisation scheme on rectangular grids with both uniform and non-uniform grid spacing in the radial coordinate. In addition, the use of localized unstructured grid refinement based on high velocity gradients in the computed solution was also explored to resolve the very high flow gradients that occur in the region of the air-water interface. However, difficulties were encountered in obtaining convergence for computations with localized grid refinement.

The grid refinement tests indicated that the flow predictions in the interface region were very sensitive to grid refinement, as has been noted in [22], whereas the cross-sectional flow profiles inside the jet, that is the main region of interest in the present work, were relatively insensitive to the choice of grid. Thus, for computational efficiency and stability, rectangular grids with non-uniformly spaced radial gridlines were used for the axisymmetric model, while relatively fine radial grid spacings were employed in the radial direction in the region of the air-water interface. To reduce the overall computer run time on a multi-processor SGI origin 3000 supercomputer, the parallel version of the Fluent flow solver was used over 4-10 compute nodes, depending on the available resources at the commencement of each run.

After a converged solution was obtained, abrasive particles were added into the pure waterjet across the inlet at various radial positions. As it is a normal expectation in an AWJ machine that particles are entrained through the mixing chamber and nozzle to the velocity close to that of the water at the nozzle exit, the initial particle velocity at the inlet was set to the velocity of its surrounding water, and the particle velocities were calculated using the Discrete Phase Model available in Fluent6.

3. RESULTS AND DISCUSSION

3.1 Dynamic characteristics of water flow field

A set of tests with different initial peak velocity of the $1/7^{th}$ power law distribution and nozzle diameters have been carried out. The CFD results for the jet flow with peak inlet velocities of 600, 700, 800 and 900m/s and nozzle diameters of 0.8, 1.0 and 1.2mm were obtained and some representative plots are given in Figs. 2 and 3.

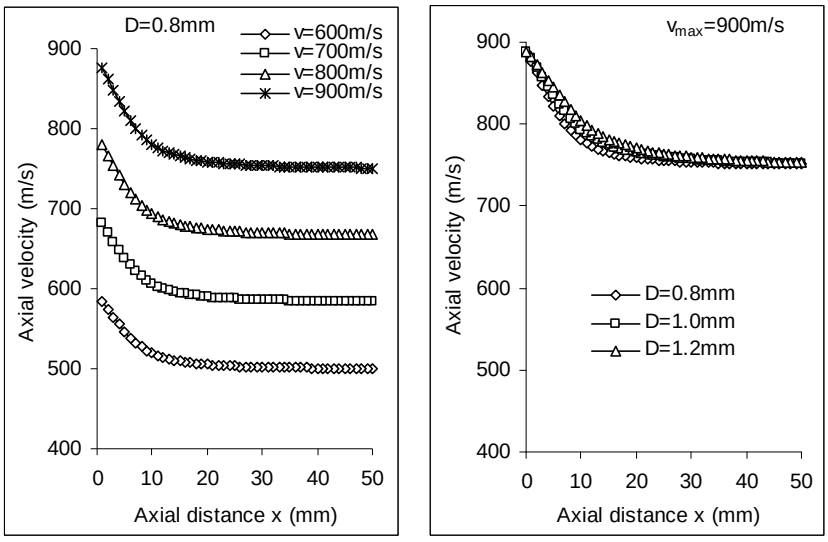

(a) (b)

Figure 2. The axial velocity of water at the jet centre vs axial distance.

Figure 2(a) shows the variation of jet axial velocity at the jet centre with the axial distance from the inlet and under different inlet peak velocities (600-900m/s). All the curves indicate that there is initial rapid decay in the jet velocity within the axial distance of approximately 15mm. Further downstream the change in the jet velocity within the domain considered is insignificant. This phenomenon may be caused by the viscosity of the fluid (water). Because there is a great velocity gradient from the jet core to the jet outer rim in the initial jet flow region, the fluid with higher velocity tends to pull that of lower velocity, so that the velocity gradient is reduced. As a

result, the velocity of the fluid close to the jet centre is decreased while that close to the jet rim is increased. It is believed that the velocity variation within the jet should follow the rule of flow mass conservation. Since the velocity gradient is reduced as the water flow away from the nozzle, the velocity change is reduced too.

Figure 2(b) shows the effect of nozzle diameters at an inlet peak velocity of 900m/s. It is noticed that a reduction in nozzle diameter corresponds to a slightly more rapid decay of the jet velocity along the jet axis in the initial region of about 20mm. Further downstream, the jet velocity for all nozzle diameters approaches approximately the same value at about 85% of the inlet peak velocity, independent of nozzle diameters.

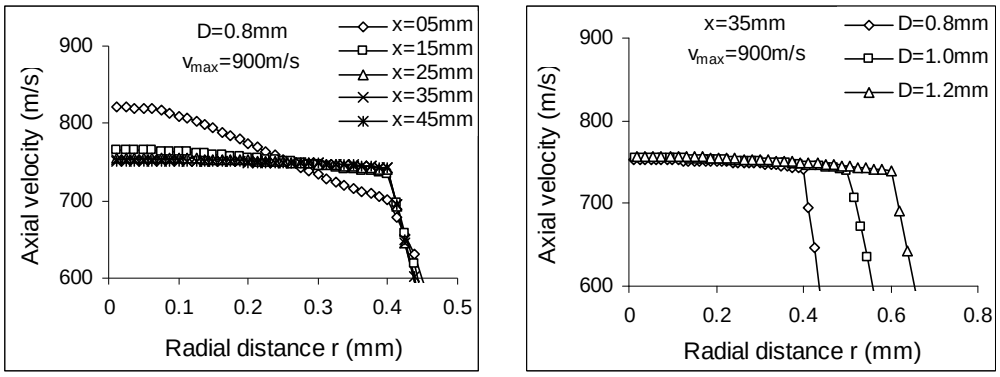

(a) (b)

Figure 3. Jet axial velocity profile in jet cross-sections.

In Figure 3(a), the jet axial velocity profiles in five cross-sections at axial distance x = 5, 15, 25, 35 and 45mm from the origin (AB) are given to illustrate the variation in jet axial velocity across and along the jet flow. The velocity profile at close to the inlet (x=5mm) again shows a rapid drop towards the jet outer rim. As mentioned above, the fluid velocity close the jet core decreases and that close to the jet outer rim increases as the jet flows. It appears that at x=15 and downstream, the velocity has approached a balanced value so that the velocity variation across the jet is minimal. Thus, the jet velocity profiles within the jet domain (when radial distance ≤0.4mm) flatten out as the distance from the nozzle exit increases, and evolve to top-hat profiles characterized by an almost constant axial velocity for $0 \le r \le D/2$. This may be a reason why kerf taper is larger in the upper than the lower region of the cutting front in AWJ cutting.

Figure 3(b) shows the influence of nozzle diameter on the jet axial velocity profile at axial location of x=35mm. It is noticed that the cross-sectional flow profile has evolved to a downstream top-hat profile that is essentially the same irrespective of the inlet nozzle diameter.

3.2 Particle velocities and trajectory

The particle shape was assumed to be spherical and the CFD study used garnet particles of four different diameters, i.e. 0.08, 0.12, 0.16 and 0.20mm. Figure 4(a) shows the particle velocity at the jet centre along the jet axis for each of the four particle sizes together with the water velocity for a comparison purpose. The particles were released at the jet centre and it was assumed that the particle velocity at the inlet is the same as that of its surrounding water. The figure indicates that the decay of particle velocities with the axial distance is in a similar way to the water velocity. Quantitatively, the water velocity decays more rapidly than the particle velocity, and small particles decelerate more quickly than large particles, as might be expected as small particles have less mass and less momentum and therefore their velocity decays more quickly.

It is noted from some predictive models in AWJ cutting [23] that the rate of volume removal is proportional to $v_p^{2.5} D_p^3$. The result in Figure 4(a) is consistent with those predictive models. It indicates that using larger grit sizes will increase the cutting efficiency because both the particle mass and velocity at a given downstream location are greater than those of small particles. This result is heartening in that it confirms that the current CFD simulation model is correct.

Figure 4(b) shows the effect of nozzle diameter, *D*, on the downstream particle velocities. The plots for the three *D*'s can almost be represented by a single curve, although at a given axial location *x/D*, a larger *D* is associated with a slightly higher particle velocity. The simulation data for the other maximum inlet velocities (600-800m/s) yield identical trends as those shown in Figure 4(b).

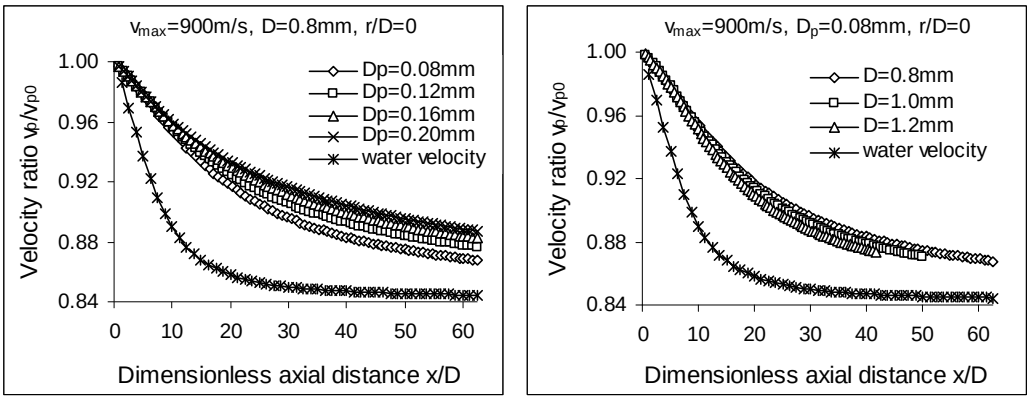

(a) (b)

Figure 4. Particle centreline velocities

It can also be noticed from Figure 4 that the downstream particle velocity approaches the corresponding jet velocity as the jet flows away. Both the particle and water velocities arrive at about 85% of the peak inlet velocity within the domain considered. The decrease in particle velocity downstream reduces the particle energy to cut the materials.

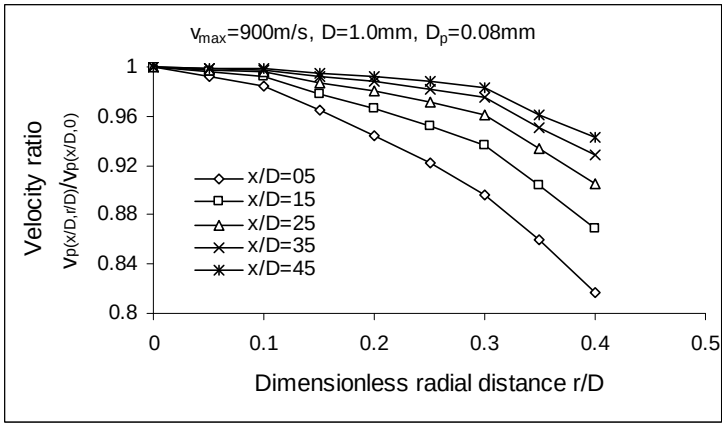

Figure 5. Particle velocity profile

The particle velocity profiles at five downstream locations *x/D*=5, 15, 25, 35 and 45 are plotted in Figure 5 for the case of v_{max}=900m/s, *D*=1mm and D_p=0.08mm. The particle velocity is represented by a velocity ratio, that is defined as the particle velocity at a dimensionless radial distance *r/D* to that at the jet centre in the same jet cross-section. The figure shows that the

particle velocity at a given cross-section decreases as the radial distance from the jet centre increases. It also shows that the rate of particle velocity decrease with the radial distance becomes smaller at locations further downstream, where the particle velocity is expected to approach a more top-hat profile inside the jet. It is anticipated that the evolution of the particle velocities from a fully developed profile at the inlet towards a more top-hat profile downstream may be related to the experimentally observed taper angle at the upper portion of a kerf produced by an AWJ followed by more parallel kerf walls at the lower part.

4. CONCLUSIONS

A CFD simulation of ultrahigh velocity waterjets and abrasive waterjets has been presented. The study has provided an in-depth understanding of the dynamic characteristics of the water and particles inside a jet. It has been shown that an AWJ has an "initial region" that is characterized by a rapid decay of the axial velocity at the jet centre. The results for the downstream velocity of the particles showed that velocity decay for different sizes of particles was similar, but less than that of the corresponding water velocity and that smaller diameter particles decelerate more rapidly than larger particles. Further, it has been shown that the particle velocities at a given jet cross-section evolve towards a more top-hat profile as the jet flows away from the nozzle. These findings are coincide with the trends extracted from the predictive models in the literature and amply explained some kerf geometrical features produced in AWJ cutting. More importantly, this study provides the essential knowledge to optimise the jet characteristics through optimising the nozzle design and process parameters, and to mathematically model the jet (and particle) characteristics for eventually modelling and improving the AWJ cutting performance.

References

[1] J. Zeng and T.J. Kim, An erosion model of polycrystalline ceramics in abrasive waterjet cutting, *Wear*, Vol. 193 (1996), 207-217

[2] H. Hocheng and K.R. Chang, Material removal analysis in abrasive waterjet cutting of ceramic plate, *J. Mater. Proc. Technol*. Vol. 40 (1994), 287-304

[3] J. Wang, *Abrasive Waterjet Machining of Engineering Materials*, Trans Tech Publications, Switzerland, (2003)

[4] E. Capello, M. Monno, Q. Semeraro and P. di Milano, Delamination in water jet cutting of multi-layered composite material. *Proc. 12th Conf. Jet Cutting Technol*. (1994), 463-476

[5] J. Wang, Abrasive waterjet machining of polymer matrix composites: Cutting performance, erosive analysis and predictive models. *Int. J. Adv. Manuf. Technol*., Vol. 15 (1999), 757-768

[6] J. Wang and D.M. Guo, A predictive depth of penetration model for abrasive waterjet cutting of polymer matrix composites. *J. Mater. Proc. Technol*.. Vol. 121/2-3 (2002), 390-394

[7] R. Kovacevic, M. Hashish, R. Mohan, et al., State of the art of research and development in abrasive waterjet machining. *J. Manuf. Sci. Eng.*, Vol. 119 (1997**)**, 776-785

[8] C.A. van Luttervelt, On the selection of manufacturing methods illustrated by an overview of separation techniques for sheet materials. *Annals of CIRP*, Vol. 38 (1989), 587-607

[9] A.W. Momber, *Principles of abrasive waterjet machining*, Springer-Verlag, London (1998)

[10] K.Yanaida, Flow characteristics of water Jets. *Proc. Symp. Jet Cutting* (1974), 20-32

[11] M. Hashish and M.P. du Plessis, Prediction equations relating high velocity jet cutting performance to stand off distance and multipasses. *J. Eng. Ind.*, Vol. 101 (1979), 311-319

[12] N.F. Neusen, T.J. Gores and R.S Amano, Axial variation of particle and drop velocities downstream from an abrasive water jet mixing tube. *Proc. 12th Conf. Jet Cutting Technol*. (1994), 93-103
[13] K.F. Neusen, D.G. Alberts and T.J. Gores, Distribution of mass in a three-phase abrasive waterjet using scanning x ray densitometry. *Proc. 10th Conf. Jet Cutting Technol*. (1990), 83-98
[14] J. Ye, R. Kovacevic, Turbulent solid-liquid flow through the nozzle of premixed abrasive waterjet. *Proc. Inst. Mech. Engrs., Part B*, Vol. 213 (1999), 59-67
[15] H.T. Liu and P. Miles, CFD and physical modelling of UHP AWJ drilling, *Proc. 14th Int. Conf. Jetting Technol*. (Belgium 1998), 15-24
[16] H. Liu, J. Wang, R.J Brown, and N. Kelson, Computational Fluid Dynamics (CFD) simulation of ultrahigh velocity abrasive waterjet. *Key engineering material*, Vols. 233-236(2003): 477-482
[17] Fluent, Fluent 6.0 User Guide, Fluent Inc
[18] G.K. Batchelor, *An introduction to fluid dynamics*, Cambridge University Press, London, (1967)
[19] B.E. Launder and D.B. Spalding, *Lectures in mathematical models of turbulence*, Academic Press, London: New York, (1972)
[20] S.A. Morsi and A.J. Alexander, An Investigation of Particle Trajectories in Two-Phase Flow Systems. *J. Fluid Mech.*, Vol.55 (2)(1972),193-208
[21] V.L. Streeter, E.F. Wylie and K.W. Bedford, *Fluid Mechanics*, WCB/McGraw Hill (1998)
[22] G. Berntsen, H. Brekke, J.O. Haugen and S. Risberg: Analysis of the free surface non-stationary flow in a Pelton turbine. *Hydropower and Dams*, Issue 6(2001), 79-84
[23] M. Hashish, A model for abrasive water jet machining. *J.Eng. Mater. Technol*, Vol.111 (1989): 154-162